Mean first passage time for a particle diffusing on a disk with two absorbing traps at the boundary

Alex Skvortsov *

Defence Science and Technology, 506 Lorimer Street, Fishermans Bend, Victoria 3207, Australia

(Received 14 February 2020; accepted 3 May 2020; published 9 July 2020)

The problem of survival of a Brownian particle diffusing on a disk with a reflective boundary that has two absorbing arcs is treated analytically. The framework of boundary homogenization is applied to calculate the effective trapping rate of the disk boundary, and this enables estimation of the mean first passage time. The method of conformal mapping is applied to transform the original system to a simpler geometrical configuration (a flat reflective boundary with a periodic configuration of identical absorbing strips) for which the analytical solution is known. The expression for the mean first passage time is simplified for some limiting cases (small arc or small gap). The derived analytical expressions compare favorably with the results of Brownian particle simulations and other analytical results from the literature.

DOI: 10.1103/PhysRevE.102.012123

I. INTRODUCTION

The problem of survival of a Brownian particle diffusing in a confined domain bounded by a reflective surface that has a small absorbing trap on it is often referred to as the narrow escape problem [1–11]. It has many applications in biology, chemical engineering, and population ecology [12–15]. The trap can represent a specific search target, an active chemical site, or an exit to the outer space from a compartment. The main parameter of interest in these studies is the mean first passage time (MFPT), i.e., the time taken for the particle to reach the absorbing trap on the boundary [1,16–18]. At the narrow escape limit, i.e., as the size of the trap decreases, the MFPT increases since it takes longer for a particle to find a smaller target. The rate of this increase depends on the dimensionality of the problem, size of the trap, and the surface morphology near the trap (locally smooth surface, corner point, bottleneck, etc. [5]). For a "regular" three-dimensional domain the MFPT increases as the inverse size of the trap, while for a two-dimensional (2D) planar domain this increase is only logarithmic [5].

Due to the mixed boundary condition on the boundary the analytical treatment of the problem is often a challenging undertaking, so only a few analytical results have been deduced in this context (for a comprehensive review, see [5] and references therein). A prominent example of such results is the solution for the MFPT for a particle diffusing inside a disk (reflective circle) with a single absorbing arc at its boundary. In addition to its canonical simplicity, this case is of methodological interest since it has become the "fundamental" solution that can be used to infer the MFPT in other planar geometries by means of conformal mapping [2]. Most of the approximate solutions derived for the narrow escape problem have been derived by employing the infinitely small target approximation. There is a variety of asymptotic methods to tackle these problems, including matched asymptotic expansions, conformal transformation, perturbation theory, and boundary homogenization [2,9,11,15,19–21].

For the case of many traps (absorbing spots) the calculation of the MFPT is more difficult, especially when the original problem cannot be simplified by applying some symmetry arguments. Indeed, the many-trap solution should account not only for the simple linear superposition of trapping rates of the individual absorbing spots but also for the implicit interaction among them (so-called many-body effects) resulting from the competition of the different traps for the same diffusing particles; the latter effect is the major difficulty in the analysis of the many-trap problem [6,7,22–24]. As a consequence, the MFPT becomes dependent not only on the size of absorbing spots but also on their relative location and mutual arrangements (clustering), and this makes analytical treatment even more challenging [22–24]. The method of boundary homogenization, which is a variation of the effective medium approach, can overcome some of these difficulties, enabling analytical progress. The aim of the method is to replace the mixed (absorbing and reflective) boundary conditions with a single uniform boundary condition imposed on the entire boundary. Such a replacement is possible because far away from a nonuniform boundary the fields of the steady-state fluxes and the concentration profile become rapidly uniform in the lateral (i.e., parallel to the boundary) direction, and these fields can be well described with a uniform boundary condition. This uniform boundary condition is formulated in terms of the Robin (radiation) boundary condition with some effective trapping rate. This trapping rate is essentially an aggregated (lumped) parameter that is completely determined by the geometrical properties of the boundary and the distribution of absorbing traps. Calculation of the trapping rate for a given geometrical setting is the critical step and the main complexity of the boundary homogenization method. It is noteworthy that there is an intrinsic analogy between the trapping rate of an absorber and the capacitance of a conductor of the same shape [18]: this analogy is based on mathematical similarity between diffusion and electrostatics and allows a simple estimation of the trapping rate of complex shape absorbers [22,25].

* alex.skvortsov@dst.defence.gov.au

It should be noted that the boundary homogenization approach, as with any effective medium theory, is only a lumped-parameter approximation. Its validity is conventionally formulated in terms of dilute configuration, i.e., the small fraction of the domain boundary occupied by absorbing traps [5,9],

$$\sigma \ll 1. \tag{1}$$

This criterion is in line with the setting for the narrow escape problem and the main rationale for the reported study. Physically, condition (1) means that a diffusing particle should be bounced many times from the reflective part of the boundary before it hits an absorbing spot (i.e., a large trapping time in comparison with the diffusion time in the domain). Nevertheless, the solution for the effective trapping rate derived below has the correct limit for $\sigma \to 1$ (i.e., for the fully absorbing boundary), so the specific threshold value of σ above which the method of boundary homogenization becomes invalid should be established numerically. As has been found by numerical simulations [11] and supported by the current study, this method can still provide reasonable estimations of the MFPT even when σ is not infinitesimally small.

Consider a particle diffusing inside a disk with a reflective boundary with a number of absorbing arcs (traps) on it. Assume we seek to replace the nonuniform boundary condition at the boundary by a uniform radiation boundary condition with some effective trapping rate κ that would provide the same trapping capacity as the all traps [21]. As a result, the problem becomes one-dimensional. The mean lifetime $\tau(r)$ of a particle that starts at distance r from the center of the disk of radius R with a uniform partially absorbing boundary satisfies the equation $d[rd\tau(r)/dr]/dr = -r/D$ with radiation boundary conditions at the disk boundary $d\tau(r)/dr = -\kappa\tau(r)/D$ and $d\tau(r)/dr = 0$ at the disk center [11,20]. Solving this equation, we can find that the MFPT is

$$\tau(r) = \frac{R^2 - r^2}{4D} + \frac{R}{2\kappa}, \tag{2}$$

which is the sum of the MFPT to the disk boundary, $(R^2 - r^2)/(4D)$, and the mean lifetime of the particle that starts from the boundary, $R/(2\kappa)$. Averaging $\tau(r)$ over the starting point, assuming that the starting point is uniformly distributed over the disk, we obtain the averaged lifetime $\langle\tau\rangle = (2/R^2)\int_0^R \tau(r) r dr$ [11,20]:

$$\langle\tau\rangle = \frac{R^2}{8D} + \frac{R}{2\kappa}. \tag{3}$$

Without the specification of trapping rate κ, this formula is valid for any configuration of absorbing traps. Below we will be using the terms "absorbing arcs" and "traps" interchangeably. The particular expression for κ should account for the size of the arcs and their mutual arrangement [9,22,23]. For the case of a single absorbing arc of length l the trapping rate is given by the formula [9,20,21]

$$\kappa = \frac{D}{2R\ln[1/\sin(\pi\sigma/2)]}, \tag{4}$$

where $\sigma = l/(2\pi R)$ is the fraction of the circle boundary occupied by the arc. This expression, as well as the expression for $\langle\tau\rangle$, Eq. (3), logarithmically diverges as $\sigma \to 0$, in line with the aforementioned general properties.

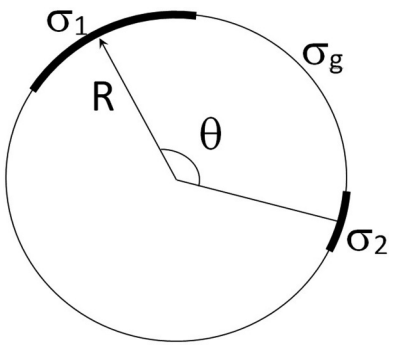

FIG. 1. Two absorbing traps at the boundary of a circular domain: σ_1, σ_2 are the fractions of domain boundaries occupied by traps, and σ_g is the fraction of the gap between the traps.

For the case of many absorbing arcs the expression for κ has been determined only for a few particular configurations. For the case of n identical and equally spaced arcs each of length l the expression for κ is still given by Eq. (3), but with [9,20,21]

$$\kappa = \frac{nD}{2R\ln[1/\sin(\pi\sigma/2)]} \tag{5}$$

and

$$\sigma = \frac{nl}{2\pi R}. \tag{6}$$

The trapping rate is a nonlinear function of n due to intertrap interaction (a signature of many-body effects). The trapping rate, Eq. (5), tends to infinity (i.e., the boundary becomes fully absorbing) in two limiting cases: (i) when $\sigma = 1$ and (ii) when $n \to \infty$ (for a given σ).

For the case of two identical arcs in an arbitrary location on the reflective circle (Fig. 1), an approximate formula for κ was proposed in Ref. [11] based on the numerical data fit. The same case was treated analytically in Ref. [9], where, under the "large intertrap gap" assumption, the expression for $\tau(0)$ was derived (Eq. (3.5) of Ref. [9]) that allows one to deduce the following expression for the effective trapping rate:

$$\kappa = \frac{D}{R}\left[\ln\left(\frac{2}{\pi\sigma}\right) - \ln\sin\left(\frac{\theta}{2}\right)\right]^{-1}. \tag{7}$$

Here θ is the minimal polar angle between the centers of the arcs, so $0 \leqslant \theta \leqslant \pi$ (see Fig. 1). For $\theta \to \pi$, $\kappa \to (D/2R)/\{\ln[2/(\pi\sigma)]\}$, in agreement with Eq. (4).

The aim of this paper is to derive an analytic expression for the effective trapping rate κ for the general configuration of two absorbing arcs on the reflective disk, viz., of different lengths and arbitrary separations, as shown in Fig. 1. This expression, together with Eq. (3), leads to an analytical estimation of the MFPT.

II. MAIN RESULTS

We have found that for the general configuration of two absorbing arcs, parameter κ in Eq. (3) is given by the formula

$$\kappa = \frac{D}{2R}\frac{1}{\ln(1/F)}, \tag{8}$$

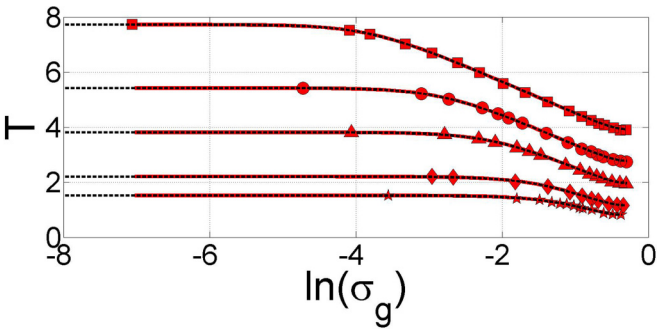

FIG. 2. The dimensionless MFPT, Eq. (26), for two identical arcs as a function of the interarc distance: Eq. (8) (solid line), asymptotic formula (7) (dashed line), and Brownian particle simulations [11] (markers as in the original paper). The different lines correspond to the different values of the boundary fraction occupied by arcs σ: $0.001/\pi$, $0.01/\pi$, $0.05/\pi$, $0.25/\pi$, $0.5/\pi$ (from top to bottom).

where $F = F_1F_2$, with

$$F_1 = \sin[\pi(\sigma_1 + \sigma_2 + \epsilon\sigma_g)/2], \tag{9}$$

$$F_2 = \cos(S/2), \tag{10}$$

and

$$S = \arcsin[\sin(\pi(\sigma_1 - \sigma_2 + \epsilon\sigma_g)/2)/F_1] - \arcsin[\sin(\pi(\sigma_1 - \sigma_2 - \epsilon\sigma_g)/2)/F_1]. \tag{11}$$

Parameters σ_1, σ_2 are the length fractions of the absorbing arcs, and σ_g is the length fraction of the smallest reflection gap between them, so that

$$\sigma_1 + \sigma_2 + \sigma_g \leqslant 1, \tag{12}$$

and $\epsilon = I(\sigma_1\sigma_2)$, with $I(\xi) = 0$ if $\xi = 0$ and $I(\xi) = 1$ otherwise.

It can be seen that this expression reduces to other cases discussed above. More specifically, for the case of either $\sigma_1 = 0$ or $\sigma_2 = 0$ we recover Eq. (4) since $\epsilon, S = 0$. The expression is also valid for the case $\sigma_g = 0$ (no gap between absorbing arcs) for which $S = 0$. For two identical arcs in antipodal locations Eq. (8) reduces to Eq. (6) with $n = 2$ (see the proof in the Appendix).

For two identical arcs in arbitrary locations the expression for κ reduces to Eq. (8) with

$$F = \{\sin^2[\pi(\sigma + \sigma_g)/2] - \sin^2(\pi\sigma_g/2)\}^{1/2}, \tag{13}$$

where $\sigma = \sigma_1 + \sigma_2$. This solution is also approximately valid for the case $|\sigma_1 - \sigma_2| \ll \sigma_g$, i.e., when the difference in length between the arcs is much smaller than the gap between them. Below, Eqs. (8), (10), and (13) will be compared with asymptotic expression (7). A comparison with Eq. (7), the case of two equal arcs in an arbitrary location, is presented in Fig. 2.

With an increase of parameter σ_g from $\sigma_g = 0$ (touching arcs) to its maximum value $\sigma_g = 1/2 - \sigma$ (two arcs in antipodal locations), we recover a universal intermediate asymptotic for $\sigma \ll \sigma_g$:

$$\kappa = \frac{D}{R}\frac{1}{\ln\eta}, \quad \eta \simeq \frac{1}{\sin(\pi\sigma/2)\sin(\pi\sigma_g)}. \tag{14}$$

By substituting it in Eq. (3) we arrive at the expression for the MFPT,

$$\langle\tau\rangle = \frac{R^2}{D}\left(\frac{1}{8} + \frac{1}{2}\ln\eta\right), \quad \sigma_g \gg \sigma. \tag{15}$$

Therefore, at this limit the MFPT slowly (logarithmically) decreases with the increase of the width of the interarc gap and length of absorbing arcs (see numerical results below).

The functional form of Eq. (15) enables the deduction of a simple "product rule" for the MFPT: it is the same for the configurations with the same product $\sin(\pi\sigma/2)\sin(\pi\sigma_g)$. This law provides a simple way for comparing the MFPT for the different two-arc configurations by translating them to the equivalent two-equal-arc configuration in antipodal locations with aggregated length fraction $\sigma_e = \arcsin[(2/\pi)\sin(\pi\sigma/2)\sin(\pi\sigma_g)]$. Obviously, the length fraction of the equivalent single arc σ_e that corresponds to the same MFPT is given by the formula $\sigma_e = \arcsin[(2/\pi)\sqrt{\sin(\pi\sigma/2)\sin(\pi\sigma_g)}]$.

Equation (8) also provides insights into the effect of the difference in arc size on the trapping rate of the disk boundary and the MFPT. Formally, the difference $\sigma_1 - \sigma_2$ appears only in the argument of function F_2. If $|\sigma_1 - \sigma_2| \ll \sigma_g$, this difference can be dropped from the argument, and we return to the case of two equal arcs considered above (with combined fraction $\sigma = \sigma_1 + \sigma_2$). Similarly, in the opposite limit, when $|\sigma_1 - \sigma_2| \gg \sigma_g$, the parameter σ_g can be disregarded, resulting in the condition $F_2 = 1$, which is valid for the single-arc configuration. This implies that in the latter case two arcs act as a single arc of the combined length, so κ and hence the MFPT become independent of individual arc lengths provided the sum $\sigma = \sigma_1 + \sigma_2$ is preserved. With an increasing interarc gap solution (8) describes a smooth transition between the one- and two-arc approximations, as expected from intuitive arguments.

III. THEORETICAL FRAMEWORK

A. Displacement length

The concept of displacement length (also known as blockage length [26], slip length [27], or boundary offset [28,29]) naturally emerges in the method of boundary homogenization when applied to the problems of Laplacian transport and has been explained in detail in a number of publications [11,26–31]. There is a direct connection between displacement length and the effective trapping rate from Eq. (2), as shown below.

Displacement length is introduced when the original inhomogeneous boundary is conceptually replaced by an effective homogeneous boundary. This replacement leads to the important question about the position of the homogeneous boundary that preserves the lumped parameter of the systems (heat flux, electric current, momentum). Displacement length is simply the offset of the position of the effective homogeneous boundary from the original inhomogeneous boundary [27–30,32].

To relate displacement length and effective trapping rate it is instructive to analyze diffusive transport near a flat inhomogeneous boundary by employing the following simplified model. Consider a steady-state diffusion of particles

in a 2D plane layer (strip) of thickness H. In this case the concentration of particle obeys the 2D Laplace equation,

$$\frac{\partial^2 C}{\partial x^2} + \frac{\partial^2 C}{\partial y^2} = 0, \tag{16}$$

where x, y are Cartesian coordinates, y is the coordinate normal to the layer, and $y = 0$ corresponds to the bottom boundary. Assume that the bottom boundary of the layer is absorbing $C(y = 0) = 0$ and the top boundary is kept at constant concentration $C(y = H) = C_H = \text{const}$. Then the solution of Eq. (16) takes the form

$$C = (j_0/D)y, \tag{17}$$

where $j_0 = DC_H/H = \text{const}$ is the flux in the system.

Next, we modify the bottom boundary by introducing a periodic pattern of reflective intervals (assuming that the period of this pattern is much smaller than H). This pattern will affect the concentration profile and diffusion flux to the modified boundary. At distances far away from the bottom boundary (but still much less than H) the lateral component of the flux rapidly decreases, leading to the following saturation profile of the particle concentration:

$$C = (j_0/D)(y + \Delta), \tag{18}$$

involving a parameter $\Delta \geqslant 0$ called displacement length [28–30,32].

Parameter Δ is the only signature of the boundary modification (since for the original boundary $\Delta = 0$). The analytical expression for Δ can be deduced from the solution of the Laplace equation (16) and is specific to a particular boundary. Importantly, that Δ in any case is determined only by geometrical parameters of the inhomogeneous boundary and is independent of particle concentration (this comes from the linearity of the Laplace equation and boundary conditions). Displacement length completely determines the modified flux in the system, $j = j_0/(H + \Delta)$, since now $C = 0$ at $y = -\Delta$ and not at $y = 0$.

It is well known (see [11,20] and references therein) that the boundary consisting of a periodic pattern of absorbing and reflective intervals can be characterized by a radiation boundary condition,

$$D\frac{\partial C}{\partial y} = \kappa C, \tag{19}$$

with some effective trapping rate κ. The limits $\kappa = 0$ and $\kappa = \infty$ in this boundary condition correspond to the fully reflective and absorbing boundaries, respectively.

By substituting Eq. (18) into Eq. (19) we can deduce a simple relation between parameters κ and Δ:

$$\kappa = D/\Delta. \tag{20}$$

Equation (20) implies that if, for a given inhomogeneous boundary, we manage to deduce the far-field limit of the solution of the Laplace equation in the form of Eq. (18), we can identify displacement length Δ and then from Eq. (19) obtain the effective trapping rate κ in the radiation boundary condition. The trapping rate according to Eq. (3) leads to calculation of the MFPT.

In the context of the two-trap problem, Fig. 1, we apply the same framework to the solution of the Laplace equation for a disk with two absorbing arcs at its boundary and impose the far-field limit, Eq. (18), in a circular domain. To this end we employ the method of conformal transformation.

B. Conformal transformation

To illustrate the main idea of the method we begin with solution (17) for a 2D layer with the perfectly absorbing boundary at $y = 0$:

$$C(x, y) = (j_0/D)\,\mathrm{Im}(z), \tag{21}$$

where $z = x + iy$ is complex coordinate. Under the conformal map $\omega = \omega(z) = u + iv$, which transforms the original boundary at $y = 0$ to a more complex boundary (with nonuniform absorbing properties or geometrical profile), this solution becomes

$$C(x, y) = (j_0/D)\,\mathrm{Im}[\omega(z)]. \tag{22}$$

Then, by imposing the far-field limit, $y \to \infty$, we expect $\omega(z) \simeq z + i\Delta$, where Δ is real, and we can identify displacement length Δ.

Next, we transform solution (22) to a circular domain. Assuming periodicity along the layer with period $2\pi R$, we apply conformal map $\omega/R = \exp(iz/R)$ and transform a period of the layer [a rectangle $0 \leqslant x \leqslant 2\pi R$, $0 \leqslant y \leqslant H$ onto an annulus $a \leqslant |\omega| \leqslant R$, $a = R\exp(-H/R)$]. The internal radius of the annulus a, where the concentration of particles is kept constant $C = C_H$, is relatively small ($a \ll R$) because H is much larger than the period $2\pi R$, as initially assumed. If the bottom boundary of the layer has a periodic pattern of absorbing and reflective intervals, this map transforms this pattern into a pattern of absorbing and reflective arcs on the external circle, preserving their relative fractions. Importantly, if we apply the boundary homogenization approach to the inhomogeneous bottom boundary of the layer and replace it with the uniform partially absorbing boundary with some effective trapping rate κ, this trapping rate will be the same as for the external boundary of the annulus. This property is due to the preservation of total flux under conformal transformation [33] and the total length of the external boundary (for details, see [20]). From the equality of the two trapping rates immediately follows the equality of displacement lengths, Eq. (20), and this enables us to perform calculations of Δ in the rectangular domain with two reflective side boundaries, the top boundary at $y = H$, where $C = C_H = \text{const}$, and the bottom boundary at $y = 0$, which has reflective base with two absorbing intervals (see Fig. 3).

As the next step we transform the inhomogeneous boundary at $y = 0$ to the perfectly absorbing boundary by "removing" reflective parts between absorbing intervals and vertical reflective boundaries of the rectangle (Fig. 3). We rescale the width of the rectangle, so it becomes $-\pi/2 \leqslant x \leqslant \pi/2$. We can always select the position of the period such that the reflective intervals adjacent to the vertical walls become equal. Then we apply the mapping function [30,32,34,35]

$$\omega(z) = \arccos[F\cos(z)], \tag{23}$$

where the parameter F is a constant and is initially undefined. This transformation maps the elongated rectangular domain (actually, strip $-\pi/2 \leqslant x \leqslant \pi/2$, $y > 0$) onto itself

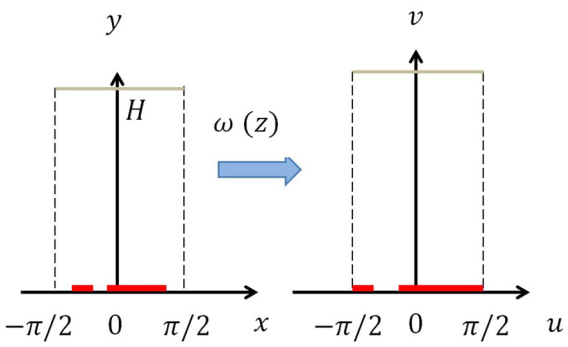

FIG. 3. The result of transformation (23) for some value of parameter F.

and stretches its boundary. The value of the "stretch" parameter F can be selected in a special way so that the ends of absorbing intervals at the bottom after transformation will be located at the ends of the period adjacent to the vertical walls. Therefore, the transformation (23) essentially removes the reflective gaps adjacent to the vertical boundaries of the period [30,32,34,35] (see Fig. 3). In a similar manner, if applied recursively (shifting the origin after each step), this transformation can remove any number of reflective gaps from the absorbing boundary, resulting in the perfectly absorbing boundary located at $y = 0$. It also shifts the position of the top boundary, and this shift is equal to Δ [32] (for more details see [30,32]).

An important property of mapping (23) is its preservation of the functional form for subsequent applications and for inverse transformation (it changes only the stretch parameter β). For the case of two absorbing intervals the result reads

$$F = F_1 F_2, \tag{24}$$

where F_1, F_2 are given by Eqs. (9) and (10).

By reinstating dimensional variables, substituting Eqs. (23) and (24) into (22), applying the identity $\arccos z = -i \ln(z + i\sqrt{1-z^2})$, and taking limit $y \to \infty$, we derive the following expression for displacement length:

$$\Delta = -\ln(F_1 F_2). \tag{25}$$

Finally, by using Eq. (20) we arrive at the main result, Eq. (8).

IV. NUMERICAL VALIDATION

For validation we compare the above analytical results with some asymptotic formulas and Brownian particle simulations [11]. We plot the mean particle lifetime, Eqs. (7) and (8), measured in the diffusion time units, R^2/D,

$$T = \langle \tau \rangle \frac{D}{R^2} = \frac{1}{8} + \ln\left(\frac{1}{F}\right), \tag{26}$$

where for κ we use Eq. (8). The right-hand side of this equation is a dimensionless function and depends only on fractions $\sigma_1, \sigma_2, \sigma_g$.

First, we present results for the dimensionless MFPT, Eq. (26), for the configuration of two identical arcs in arbitrary locations. In Fig. 2 we depict the plot of the MFPT as a function of the gap between the arcs. Motivated by Eqs. (14) and (15), we use $\ln(\sigma_g)$ as a variable so that the intermediate asymptotic (14) corresponds to the straight lines (assuming $\sigma_1, \sigma_2, \sigma_g \ll 1$). The thick solid lines are the solution given by Eq. (8), the markers are the results of Brownian particle simulations [11], and the dashed lines are the asymptotic formula (7). We observe excellent agreement between all data sets for the broad range of the absorbing-arc fraction, $0.001/\pi \leqslant \sigma \leqslant 0.5/\pi$, where $\sigma = \sigma_1 + \sigma_2$. Generally speaking, formula (7), being developed for the well-separated configurations, is not directly applicable for the small-gap limit (it logarithmically diverges as $\theta \to 0$). To overcome this issue we modified Eq. (7) with the substitution

$$\theta = \pi(\sigma_g + \sigma) \tag{27}$$

and found very good agreement with Eq. (8) and Brownian particle simulations over the broad range of the two-equal-arc configurations (the dashed lines in Fig. 2 and data in Table I). The saturation value of each line for the small σ_g limit (horizontal asymptotes) corresponds to the solution for a single arc of combined length.

TABLE I. Maximum relative error (%) for the simulation data fit. Note that all simulation results are from Ref. [11] and Fig. 2.

	σ				
	$0.001/\pi$	$0.01/\pi$	$0.05/\pi$	$0.25/\pi$	$0.5/\pi$
Eqs. (3), (7), (27)	0.45	1.14	1.51	0.75	1.06
Eqs. (3), (8)	0.45	1.14	1.50	0.64	0.42

To compare data fit, given by asymptotic formula, Eq. (7), and general solution, Eq. (26), we calculated the relative percentage error for each data point $100|T - T_{\rm sim}|/T_{\rm sim}$, where $T_{\rm sim}$ is a data point from Brownian particle simulations [11]. The maximum value of the relative error for each scenario of simulations (data series in Fig. 2) is presented in Table I.

Next, we validate the product rule predicted by Eq. (15). We plot particle simulation data from Fig. 2 as a function of one aggregated variable $\ln\eta$ along with the theoretical prediction for the dimensionless MFPT, Eq. (15): $T = 1/8 + (1/2)\ln\eta$ (Fig. 4, solid line). Only data points with $\sigma_g > \sigma$ are presented, which is the condition of validity of Eq. (15). We can conclude that the results of particle simulations agree well with the product rule over the six-decade range of the "aggregated" variable η.

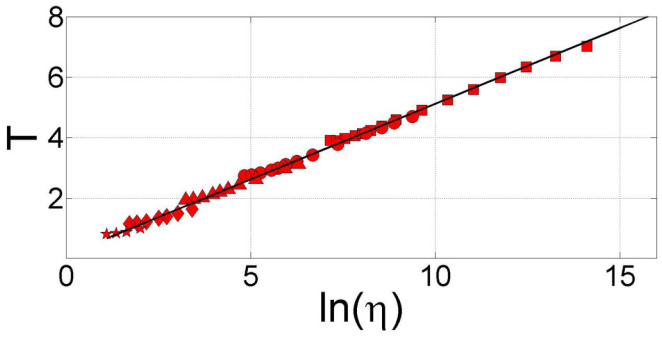

FIG. 4. The product rule for the MFPT for two identical arcs, Eq. (15) (solid line) and Brownian particle simulations [11] (markers as in the original paper and in Fig. 2).

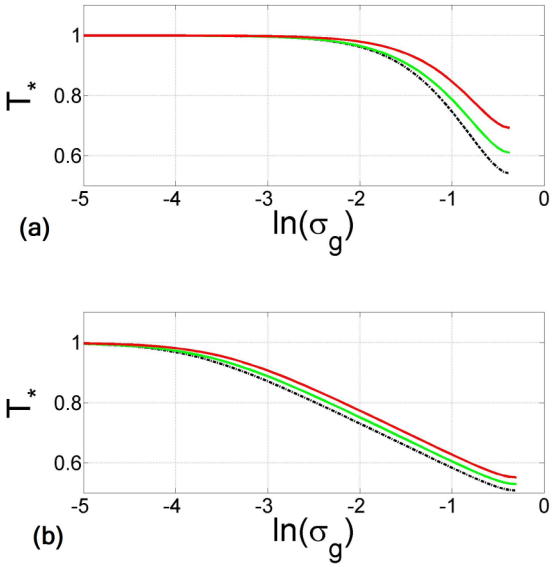

FIG. 5. The MFPT for two arcs of different lengths, σ_1, σ_2, normalized with the MFPT for a single arc of combined length $\sigma = \sigma_1 + \sigma_2$: (a) $\sigma = 0.5/\pi$ and (b) $\sigma = 0.002/\pi$. The bottom (dashed) line in each plot is $\sigma_1/\sigma_2 = 1$ (two identical arcs), the middle line is $\sigma_1/\sigma_2 = 5 \times 10^{-2}$, and the top line is $\sigma_1/\sigma_2 = 5 \times 10^{-5}$.

Finally, we investigated the effect of the difference in length of the arcs on the MFPT, as shown in Fig. 5. We use $\ln(\sigma_g)$ as a variable, so that when $\sigma, \sigma_g \ll 1$, the asymptotes of large separation given by Eq. (14) correspond to the straight lines with slope and are clearly identifiable. The values for the MFPT are normalized with the MFPT for a single arc of combined length [$T_* = T/T_1$, where T_1 is given by Eq. (26) with $\sigma_g = 0$], so all plots tend to unity for the small-gap limit. In line with the theoretical predictions, the deviation of the plots from the horizontal asymptote, which manifests a transition from the one- to two-arc approximation, occurs at $\sigma_g > \sigma$, which is clearly visible from a comparison of the two panels in Fig. 5. We also depict the MFPT for two identical arcs of the same combined length (the dashed line in Fig. 5). It can be seen that the two-equal-arc solution provides a reasonable approximation for a broad range of configurations, including an extreme asymmetry in arc length (note that the apparent origin in Fig. 5 corresponds to $T_* = 0.5$ and not to $T_* = 0$). This means that the effect of the difference in arc length is relatively weak, as predicated by the theory. Similarly, the single-arc model performs satisfactorily only in the limit of a very small gap.

For the case of two unequal absorbing arcs we could not find any published data on Brownian particle simulations to compare with our analytical predictions.

V. CONCLUDING REMARKS

In this paper we have calculated the MFPT for a Brownian particle diffusing in a disk domain with two absorbing traps at its boundary. The traps are formed by arcs of a different length with an arbitrary separation. By applying the method of boundary homogenization and conformal transformation we derived an explicit expression for the MFPT in terms of geometrical parameters of the system. We validated our analytical results with available asymptotic solutions and with Brownian dynamics simulations reported in the literature and found excellent agreement. In line with the previous studies, our results even indicate that the method of boundary homogenization can provide a reasonable estimation of the MFPT outside the very dilute approximation.

We found that the theoretical framework, employing ideas of boundary homogenization, provides a simple, yet self-consistent, framework for the analytical treatment of first passage phenomena for the case of a Brownian particle diffusing on a disk with a reflective boundary that has two absorbing traps. This approach allows us to gain some insights into the effect of relative trap size and their position. In particular, it provides an intuitively appealing approach for a simple estimation for the MFPT for an arbitrary configuration of two traps. Depending on the relative size of the intertrap gap the original configuration can be replaced with an equivalent configuration of either one or two traps (arcs) of the same aggregated length for which the analytical solutions are available.

The results of this paper also enable a simple refinement of the condition of validity of the boundary homogenization approach in the case considered. Indeed, from Eq. (26) and the requirement for the large trapping time, we arrive at the refined condition of validity

$$\ln(1/F) > 1, \tag{28}$$

where F is given in Eqs. (8)–(11). This condition was fulfilled in the numerical simulation presented in Fig. 2.

The presented approach can be generalized in two ways. Being applied iteratively, the conformal transformation (23) can be extended to treat an arbitrary number of absorbing arcs in a general configuration. Unfortunately, the analytical expressions quickly become cumbersome, but numerical treatment is straightforward. For n different absorbing arcs the MFPT is always bound by two limits, viz., its maximal value estimated for a single arc of aggregated length and its minimal value corresponding to the configuration of n equally spaced identical arcs of the same combined length.

It is also possible to get insight into the MFPT for a Brownian particle diffusing in other geometries of the domain with two absorbing traps on a reflective boundary provided a conformal transformation between a circle and the domain of interest is known. The theoretical framework for this generalization is presented in [2].

ACKNOWLEDGMENTS

The author thanks A. Berezhkovskii and I. MacGillivray for many useful discussions.

APPENDIX

Assume an antipodal configuration of two identical absorbing intervals, $\sigma_1 = \sigma_2 = \sigma/2$. By substituting it in the general solution (8) we derive

$$F_1 = \sin[\pi(1+\sigma)/4].$$

For F_2 we use Eq. (11) and conclude

$$\begin{aligned} F_2 &= \cos\left(\arcsin\left[\frac{\sin[\pi(1-\sigma)/4)]}{\sin[\pi(1+\sigma)/4]}\right]\right) \\ &= \left[\frac{\sin^2[\pi(1+\sigma)/4] - \sin^2[\pi(1-\sigma)/4]}{\sin^2[\pi(1+\sigma)/4]}\right]^{1/2} \\ &= \left[\frac{\sin^2[\pi(1+\sigma)/4] - \cos^2[\pi(1+\sigma)/4]}{\sin^2[\pi(1+\sigma)/4]}\right]^{1/2} \\ &= \left[\frac{\sin(\pi\sigma/2)}{\sin^2[\pi(1+\sigma)/4]}\right]^{1/2}. \end{aligned}$$

Therefore,

$$F = F_1 F_2 = \sqrt{\sin(\pi\sigma/2)},$$

or

$$\ln(1/F) = (1/2)\ln[1/\sin(\pi\sigma/2)].$$

From Eq. (8) it can be seen that this result corresponds to double the value of κ for a single absorbing arc, which is in agreement with Eq. (5).

[1] R. Metzler, G. Oshanin, and S. Redner, *First-Passage Phenomena and Their Applications* (World Scientific, Singapore, 2014).
[2] D. S. Grebenkov, Phys. Rev. Lett. **117**, 260201 (2016).
[3] D. S Grebenkov, R. Metzler, and G. Oshanin, New J. Phys. **21**, 122001 (2019).
[4] O. Benichou and R. Voituriez, Phys. Rev. Lett. **100**, 168105 (2008).
[5] D. Holcman and Z. Schuss, *Stochastic Narrow Escape in Molecular and Cellular Biology* (Springer, Berlin, 2015).
[6] A. Singer, Z. Schuss, and D. Holcman, J. Stat. Phys. **122**, 465 (2006).
[7] A. Singer, Z. Schuss, and D. Holcman, J. Stat. Phys. **122**, 491 (2006).
[8] Z. Schuss, A. Singer, and D. Holcman, Proc. Natl. Acad. Sci. USA **104**, 16098 (2007).
[9] S. Pillay, M. J. Ward, A. Peirce, and T. Kolokolnikov, Multiscale Model. Simul. **8**, 803 (2010).
[10] I. V. Grigoriev, Y. A. Makhnovskii, A. M. Berezhkovskii, and V. Y. Zitserman, J. Chem. Phys. **116**, 9574 (2002).
[11] A. M. Berezhkovskii and A. V. Barzykin, Phys. Rev. E **82**, 011114 (2010).
[12] P. Hanggi, P. Talkner, and M. Borkovec, Rev. Mod. Phys. **62**, 251 (1990).
[13] P. C. Bressloff and J. M. Newby, Rev. Mod. Phys. **85**, 135 (2013).
[14] H. E. Stanley, Nature (London) **401**, 12 (1999).
[15] M. Z. Bazant, Phys. Rev. Fluids **1**, 024001 (2016).
[16] S. Redner, *A Guide to First Passage Processes* (Cambridge University Press, Cambridge, 2001).
[17] O. Benichou and R. Voituriez, Phys. Rep. **539**, 225 (2014).
[18] P. L. Krapivsky, S. Redner, and E. Ben-Naim, *A Kinetic View of Statistical Physics* (Cambridge University Press, Cambridge, 2013).
[19] L. Dagdug, A. M. Berezhkovskii, and A. T. Skvortsov, J. Chem. Phys. **142**, 234902 (2015).
[20] A. T. Skvortsov, A. M. Berezhkovskii, and L. Dagdug, J. Chem. Phys. **143**, 226101 (2015).
[21] C. B. Muratov and S. Y. Svartsman, Multiscale Model. Simul. **7**, 44 (2008).
[22] A. M. Berezhkovskii, L. Dagdug, V. A. Lizunov, J. Zimmerberg, and S. M. Bezrukov, J. Chem. Phys. **136**, 211102 (2012).
[23] C. Eun, J. Chem. Phys. **149**, 024102 (2018).
[24] C. Eun, Int. J. Mol. Sci. **21**, 997 (2020).
[25] A. M. Berezhkovskii and A. V. Barzykin, J. Chem. Phys. **126**, 106102 (2007).
[26] P. A. Martin and R. A. Dalrymple, J. Fluid Mech. **188**, 465 (1988).
[27] E. Lauga, M. P. Brenner, and H. A. Stone, Microfluidics: The no-slip boundary condition, in *Handbook of Experimental Fluid Dynamics*, edited by C. Tropea, A. Yarin, and J. F. Foss (Springer, New York, 2007), pp. 1219–1240.
[28] D. Vandembroucq and S. Roux, Phys. Rev. E **55**, 6171 (1997).
[29] M. G. Blyth and C. Pozrikidis, Int. J. Heat Mass Transfer **46**, 1329 (2003).
[30] A. Skvortsov and A. Walker, Phys. Rev. E **90**, 023202 (2014).
[31] D. P. Hewett and I. J. Hewitt, Proc. R. Soc. A **472**, 20160062 (2016).
[32] A. T. Skvortsov, A. M. Berezhkovskii, and L. Dagdug, J. Chem. Phys. **150**, 194109 (2019).
[33] M. Z. Bazant, Proc. R. Soc. A **460**, 1433 (2004).
[34] W. R. Smythe, *Static and Dynamic Electricity* (Taylor and Francis, New York, 1989).
[35] J. R. Philip, Z. Angew. Math. Phys. **23**, 353 (1972).